Journal of Power Sources 231 (2013) 39–43

Contents lists available at SciVerse ScienceDirect

Journal of Power Sources

journal homepage: www.elsevier.com/locate/jpowsour

Short communication

Facile solid-state synthesis of Li_2MnSiO_4/C nanocomposite as a superior cathode with a long cycle life

Jing Liu, Huayun Xu, Xiaolei Jiang, Jian Yang*, Yitai Qian

Key Laboratory of Colloid and Interface Chemistry, Shandong University, Ministry of Education, and School of Chemistry and Chemical Engineering, Shandong University, Jinan 250100, PR China

HIGHLIGHTS

- Li_2MnSiO_4/C nanocomposite is synthesized by a facile solid-state reaction.
- The typical size of Li_2MnSiO_4 nanoparticles is in the range of 20–50 nm
- The nanocomposite exhibits a discharge capacity of 136 mAh g^{-1} after 140 cycles.
- The nanocomposite also shows a greatly improved rate performance.

GRAPHICAL ABSTRACT

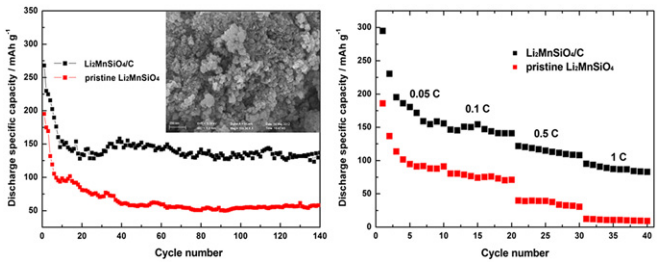

ARTICLE INFO

Article history:
Received 3 September 2012
Received in revised form
14 December 2012
Accepted 17 December 2012
Available online 24 December 2012

Keywords:
Citric acid
Solid-state reaction
Long cycle life
Nanocomposite

ABSTRACT

The Li_2MnSiO_4/C nanocomposite has been successfully synthesized at a relatively low temperature of 650 °C by a facile solid-state reaction using citric acid as the carbon source. The highly crystalline Li_2MnSiO_4 nanoparticles in the size of 20–50 nm are coated by a uniform carbon layer in a thickness of 2–5 nm. At a rate of 0.05 C, the Li_2MnSiO_4/C nanocomposite exhibits a discharge specific capacity as high as 268 mAh g^{-1} for the first cycle and a reversible capacity of about 136 mAh g^{-1} after 140 cycles at room temperature. Meanwhile, an improved rate performance is achieved by the Li_2MnSiO_4/C nanocomposite. These superior electrochemical properties could be attributed to the nanoscale particle size and the enhanced electronic conductivity.

© 2012 Elsevier B.V. All rights reserved.

1. Introduction

Lithium transition metal silicates, Li_2MSiO_4 (M = Fe, Mn and Co), have recently attracted a lot of interests as cathodes for lithium-ion batteries due to their high theoretical capacities (>300 mAh g^{-1}) and good thermal stability from strong Si–O bonding [1–3]. Among these orthosilicates, Li_2MnSiO_4 has been highlighted because of its low cost, environmentally benign and high theoretical capacity [4]. Moreover, Li_2MnSiO_4 shows a relatively high cell voltage originated from Mn^{2+}/Mn^{4+} redox couple, resulting in a much higher theoretical energy density than that of $LiFePO_4$ [5–8]. However, similar to most polyanionic materials, Li_2MnSiO_4 suffers from a slow lithium-ion diffusion rate and an extremely low electronic conductivity (5×10^{-16} S cm^{-1}) [9]. Hence, the electrochemical performance of Li_2MnSiO_4 is far away to be satisfied. For instance, Li_2MnSiO_4 synthesized through a modified Pechini sol–gel technique [2] only showed the intercalation of 0.6 mol Li per formula unit (~100 mAh g^{-1}) in the first cycle at a rate of C/30. Furthermore, this capacity quickly decreased to ~50 mAh g^{-1} after 5 cycles.

* Corresponding author. Tel./fax: +86 531 88364489.
E-mail address: yangjian@sdu.edu.cn (J. Yang).

0378-7753/$ – see front matter © 2012 Elsevier B.V. All rights reserved.
http://dx.doi.org/10.1016/j.jpowsour.2012.12.071

One strategy for the better electronic and lithium-ion transport kinetics is to reduce the particle size to the order of nanometer, which means the drastically shortened diffusion length. So, Li_2MnSiO_4 nanoparticles have been synthesized by various approaches, such as microwave solvothermal synthesis, supercritical solvothermal method, hydrothermal process, and sol–gel technique [10–14]. But many problems have been encountered in these liquid-based methods for massive production of high-quality Li_2MnSiO_4, due to the poor crystallinity, expensive equipments and complicated operation steps. These challenges could be addressed by solid-state reactions.

Surface coating of carbon as a conductive layer on Li_2MnSiO_4 has been regarded as another effective strategy to improve its electrochemical properties. Li et al. [15] developed a solution-based reflux process to synthesize the Li_2MnSiO_4/C nanocomposite using sucrose as the carbon source. The as-obtained Li_2MnSiO_4/C nanocomposite showed the intercalation/deintercalation of more than one lithium ion per formula unit for the first time in the initial few cycles (about 1.25 reversible Li in the first cycle, 209 mAh g^{-1}) at a low current density of 5 mA g^{-1}, but the capacity quickly faded within 10 cycles. Aravindan et al. [10] reported a sol–gel process for Li_2MnSiO_4/C nanoparticles using adipic acid as the carbon source. At the rate of C/20, the Li_2MnSiO_4/C nanoparticles exhibited an initial discharge capacity of 161 mAh g^{-1} and delivered a stable discharge capacity of 115 mAh g^{-1} up to 50 cycles. Aravindan et al. [6] also tested the influence of a large quantity of carbon on the electrochemical properties of Li_2MnSiO_4. It was found that the electrode with 42% ketjen black gave the best electrochemical performance. The Li_2MnSiO_4/C composite synthesized by a solid-state reaction delivered an initial discharge capacity of 160 mAh g^{-1} at a rate of C/20, and a stable discharge capacity of about 140 mAh g^{-1} after 40 cycles. Despite the significant progresses have been made in the past years, the long-term cycling performance of Li_2MnSiO_4 has not been explored before, to the best of our knowledge.

In this work, a Li_2MnSiO_4/C nanocomposite has been successfully synthesized by a solid-state reaction using citric acid as the carbon source. Citric acid is selected as the carbon source, because its decomposition could produce a carbon layer with a good electronic conductivity [16,17]. Although citric acid was ever used in the sol–gel synthesis of Li_2MnSiO_4 as the gelating agent and the carbon source [2,18–20], it has never been used in the solid-state synthesis of Li_2MnSiO_4. The obtained Li_2MnSiO_4/C nanocomposite is characterized by XRD pattern, SEM, TEM, and HRTEM images. At room temperature, the Li_2MnSiO_4/C cathode realizes a superior cycling performance with a discharge capacity of 136 mAh g^{-1} after 140 cycles at a rate of 0.05 C. To the best of our knowledge, this is the longest cycle life for Li_2MnSiO_4-based electrodes to date, and this method is likely to be applied for industrial production.

2. Experimental methods

2.1. Preparation of the Li_2MnSiO_4/C nanocomposite

The Li_2MnSiO_4/C nanocomposite was synthesized from a solid-state reaction. In a typical synthesis, 2.1525 g of $LiOH·H_2O$ (aladdin, AR) was dissolved in a minimal amount of deionized water. Then, 2.0125 g of citric acid, 1.5 g of SiO_2 (cabosil M5) and 6.125 g of $Mn(CH_3COO)_2·4H_2O$ (aladdin, AR) were added into the solution of LiOH. The obtained slurry was ball-milled and then dried in an oven at 80 °C, producing a brown precursor. The precursor was heated to 350 °C for 1 h and then at 650 °C for 10 h under a flow of H_2(5%)/Ar(95%). The final black powder was collected for structure characterization and electrochemical measurements. In order to clarify the role of citric acid on the product, the similar processes were applied for Li_2MnSiO_4.

2.2. Physical characterization

Thermal gravimetric-differential scanning calorimetry (TG-DSC) analysis for the precursor was conducted on a Mettler Toledo TGA/SDTA851 thermal analyzer under nitrogen atmosphere. Powder X-ray diffraction (XRD) patterns were collected with a Bruker D8 Advance diffractometer using Cu Kα radiation. The particle morphology was observed by scanning electron microscopy (SEM, JEOL JSM-7600F), transmission electron microscopy (TEM, JEM-1011) and high resolution transmission electron microscopy (HRTEM, JEOL-2100).

2.3. Electrochemical measurements

The electrochemical performance of the two samples was characterized by coin-type cells (CR 2032) with lithium metal as the counter electrode. The slurry composed of 50 wt.% host material, 40 wt.% carbon black and 10 wt.% polyvinylidene fluoride (PVDF) dispersed in *N*-methylpyrrolidinone (NMP) was coated on an Al foil and dried at 80 °C under vacuum. The resulting film with the loading of host material at 2–5 mg cm^{-2} was pressed, punched into the discs with a diameter of 14 mm and used as the cathode. Celgard 2300 was used as a separator. The electrolyte was 1 M $LiPF_6$ in a mixture of ethylene carbonate (EC), diethyl carbonate (DEC) and ethyl methyl carbonate (EMC) (1:1:1 volume). All cells were assembled in an argon-filled glove box and tested at room temperature over the voltage range 1.5–4.8 V. Electrochemical impedance spectroscopy (EIS) was carried out on an electrochemical workstation (Materials Mates 510, Italia) in the frequency range from 0.1 MHz to 0.01 Hz. 1 C = 330 mA g^{-1}.

3. Results and discussion

TG and DSC analysis are conducted to give an appropriate reaction temperature for Li_2MnSiO_4/C from the precursor. As shown in Fig. 1, the weight loss of the precursor mainly happens before 500 °C. The small weight loss from 40 to 230 °C is probably due to the elimination of the absorbed water and the crystal water. The huge weight loss can be associated with the reaction of citric acid, SiO_2, $Mn(CH_3COO)_2$ and LiOH at a high temperature. In order to make sure the complete reaction, the reaction temperature for Li_2MnSiO_4 is set at 650 °C.

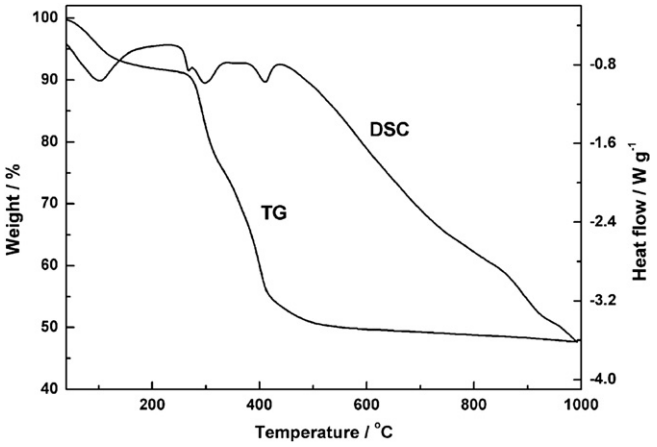

Fig. 1. TG-DSC curves for the precursor recorded from 40 to 1000 °C at a heating rate of 10 °C min^{-1} under nitrogen atmosphere.

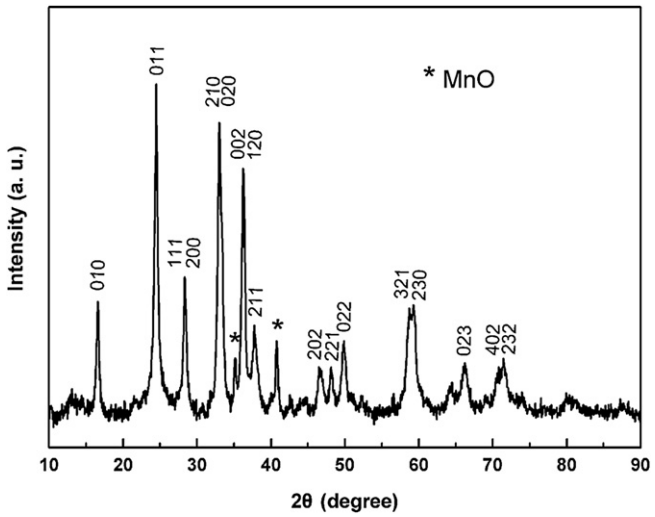

Fig. 2. XRD pattern of the Li_2MnSiO_4/C nanocomposite synthesized at 650 °C.

Fig. 2 displays the XRD pattern of the prepared Li_2MnSiO_4/C composite treated at 650 °C. The main peaks are assigned to the orthorhombic Li_2MnSiO_4 with a space group of $Pmn2_1$ [21,22], the most stable structure for Li_2MnSiO_4 [23]. However, the diffraction peaks of carbon are not observed, due to the low proportion in the product. Some peaks from MnO are presented in the diffraction pattern, which has been also reported in many literature [2,5–10,21,22].

The SEM image of the prepared Li_2MnSiO_4/C nanocomposite (Fig. 3A) shows a large number of agglomerated nanoparticles. In order to identify the size and shape of the nanoparticles, the TEM images are acquired to give a close view on them. As shown in Fig. 3B, the typical size of the nanoparticles is in the range of 20–50 nm, comparable to those of the nanoparticles obtained by the solution-based synthesis like sol–gel processes [19,22] or solvothermal methods [12,14]. This size is much smaller than that of Li_2MnSiO_4/C powder also prepared by solid-state reaction (~1 μm) [24]. This result can be attributed to the low reaction temperature in our case. The successful carbon coating on Li_2MnSiO_4 nanoparticles is evidenced by HRTEM images, as shown in Fig. 3C and D. It is found that the carbon layer is well coated on the surface of highly crystalline Li_2MnSiO_4 nanoparticles in a thickness of 2–5 nm. Since the carbon layer is *in-situ* formed by the pyrolysis of citric acid, it also effectively inhibits the growth of Li_2MnSiO_4 nanoparticles. The nanoscale size of Li_2MnSiO_4 shortens the pathways for rapid electronic and lithium-ion transfer. The conductive carbon coating connects the neighboring nanoparticles, providing highly conductive channels for electron mobility between contiguous Li_2MnSiO_4 nanoparticles [14].

Galvanostatic charge and discharge measurements of the Li_2MnSiO_4/C nanocomposite are carried out to reveal its performance as a cathode of lithium-ion batteries. Meanwhile, the electrochemical performance of the pristine Li_2MnSiO_4 is also tested for a comparison. It should be pointed out that the charge/discharge capacities of the nanocomposite are derived from the mass of Li_2MnSiO_4/C. Fig. 4A presents the typical charge/discharge curves of the Li_2MnSiO_4/C nanocomposite and the pristine Li_2MnSiO_4 at a rate of 0.05 C during the initial 5 cycles. The Li_2MnSiO_4/C nanocomposite shows a very high charge capacity during the 1st cycle, far beyond the theoretical capacity of Li_2MnSiO_4 at 333 mAh g^{-1}. Then, the initial discharge capacity of Li_2MnSiO_4/C quickly drops to 268 mAh g^{-1}, corresponding to the extraction of about 1.6 lithium ions per formula unit. The huge irreversible capacity loss may be related with the formation of solid electrolyte interphase (SEI) film [10], or the decomposition of electrolyte under the high voltage (>4.5 V). The similar behavior has been also observed by many groups [10,19,25]. Despite the crystal structure of Li_2MnSiO_4 has been destroyed after the first charge [26], the Li_2MnSiO_4/C nanocomposite still shows a large discharge capacity of 230 mAh g^{-1} for the 2nd cycle, and this value gradually decreases to ~203 mAh g^{-1} for the 5th cycle. In the case of the pristine Li_2MnSiO_4, the discharge

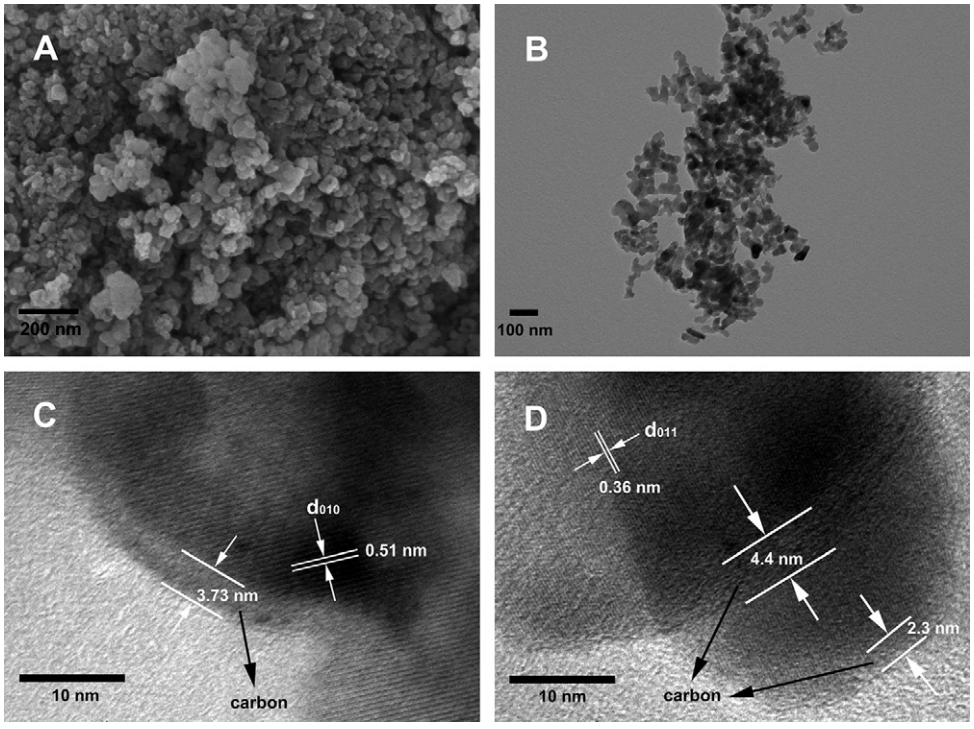

Fig. 3. SEM (A), TEM (B) and HRTEM (C and D) images of the prepared Li_2MnSiO_4/C nanocomposite.

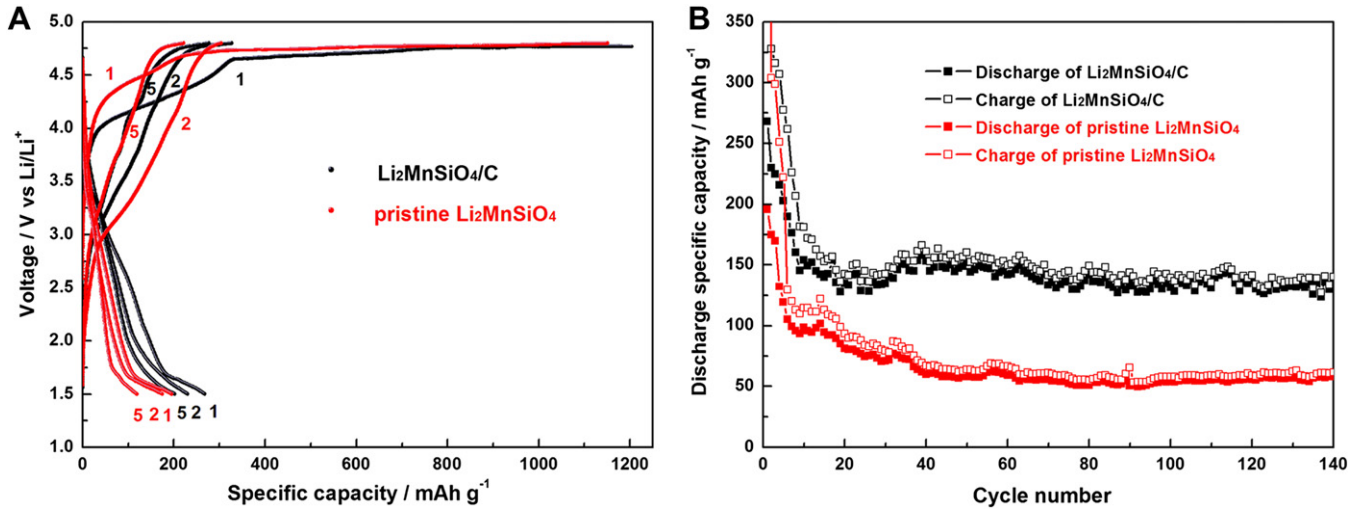

Fig. 4. Typical charge–discharge curves for the initial 5 cycles (A) and cycling performance (B) of the Li_2MnSiO_4/C nanocomposite and the pristine Li_2MnSiO_4.

capacity is ~ 196 mAh g^{-1} for the first cycle, ~175 mAh g^{-1} for the 2nd cycle and ~119 mAh g^{-1} for the 5th cycle, much lower than the counterparts in the case of the Li_2MnSiO_4/C nanocomposite. In Fig. 4B, it is found that the Li_2MnSiO_4/C nanocomposite exhibits the discharge capacities of 153 mAh g^{-1} and 152 mAh g^{-1} for the 40th and 50th cycles, respectively. These results are higher than most reported discharge capacities for Li_2MnSiO_4-based electrodes [6,10,24,27]. At the end of 140 cycles, the Li_2MnSiO_4/C cathode shows a relatively high discharge capacity of 136 mAh g^{-1}, whereas the pristine Li_2MnSiO_4 exhibits only 58 mAh g^{-1}.

Fig. 5 shows the rate capabilities of the Li_2MnSiO_4/C nanocomposite and the pristine Li_2MnSiO_4. The charge and discharge current densities are varied from 0.05 C to 1 C. As the current density increases, the discharge capacities of both samples remarkably decrease. However, it is obvious that the Li_2MnSiO_4/C nanocomposite retains much higher discharge capacities than the pristine Li_2MnSiO_4 at various rates. The superior cycling performance demonstrates that the structural instability of Li_2MnSiO_4 is restrained to a certain extent by the well-coated carbon layer on the surface of Li_2MnSiO_4 particles. In other words, the carbon layer plays a role of buffer during the structure transform process from Li_2MnSiO_4 to $MnSiO_4$. In addition, the carbon layer coated on the Li_2MnSiO_4 nanoparticles provides rapid transfer channels for the electrons during the charge–discharge process, thus leading to the enhancement of the rate performance.

Electrochemical impedance spectroscopy (EIS) was employed to distinguish the resistances in the cells. Fig. 6 shows the Nyquist plots of the impedance spectra for the Li_2MnSiO_4/C and the pristine Li_2MnSiO_4 electrodes. Both Nyquist plots typically consist of a semicircle in the high-to-medium frequency region and a slope line in the low frequency region. The semicircle can be attributed to the resistance related to the charge transfer between the electrolyte and active material, and the slope line is related with the Li^+ diffusion (Warburg diffusion) in the electrode bulk. In the inset of Fig. 6, an equivalent circuit is proposed to fit the impedance spectra of the Li_2MnSiO_4/C and the pristine Li_2MnSiO_4 electrodes. In this equivalent circuit, R_Ω and R_{ct} represent the internal resistance of the battery and the charge-transfer resistance. C_d represents the double-layer capacitance. Z_ω is the Warburg diffusion impedance. The fitting R_{ct} of the prepared Li_2MnSiO_4/C electrode (44.1 Ω) is much smaller than that of the pristine Li_2MnSiO_4 electrode (95.5 Ω), suggesting the facile lithium-ion interfacial charge transfer and then the improved

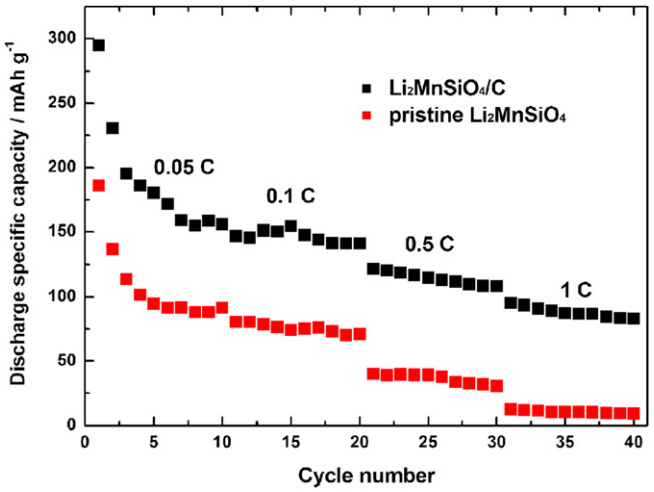

Fig. 5. Rate performances of the Li_2MnSiO_4/C nanocomposite and the pristine Li_2MnSiO_4.

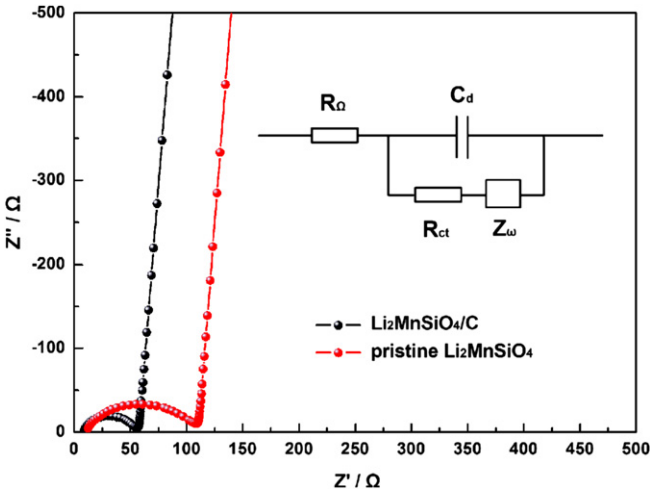

Fig. 6. Nyquist plot of the impedance spectra of the Li_2MnSiO_4/C nanocomposite and the pristine Li_2MnSiO_4.

electrochemical performance. All the above results confirm the higher reversible capacity, better cycling performance and rate capability of the Li_2MnSiO_4/C nanocomposite than the pristine Li_2MnSiO_4. Such an excellent electrochemical performance should be attributed to the short lithium-ion diffusion path, well coated carbon layer and the improved electronic conductivity.

4. Conclusions

Li_2MnSiO_4/C nanocomposite with the size over 20–50 nm has been prepared by a facile solid-state reaction using citric acid as the carbon source. XRD pattern and TEM images validate the formation of well-crystallized Li_2MnSiO_4 nanoparticles coated with a carbon layer in a thickness of 2–5 nm. The Li_2MnSiO_4/C nanocomposite shows excellent electrochemical performance, including a discharge capacity of 268 mAh g^{-1} for the first cycle, and 136 mAh g^{-1} after 140 cycles. The rate performance of the Li_2MnSiO_4/C nanocomposite is also greatly improved in comparison with that of the pristine Li_2MnSiO_4. The enhanced electrochemical performances can be assigned to the nanoscale particle size and the improved electronic conductivity induced by carbon coating. We believe the electrochemical performance of Li_2MnSiO_4 can be further improved, since much fewer efforts have been devoted on it in comparison to $LiFePO_4$.

Acknowledgments

This work is partially supported by National Natural Science Fund of China (No. 91022033, 21203111), the 973 Project of China (No. 2011CB935901), Shandong Provincial Natural Science Foundation for Distinguished Young Scholar (JQ201205), Independent Innovation Foundation of Shandong University (No. 2012 ZD007), and start-up funding for new faculties in Shandong University. J. Liu. thanks the financial support from China Postdoctoral Science Foundation (No. 2012M511490), and the Special Fund for Postdoctoral Innovation Program of Shandong Province (No. 201102022).

References

[1] A. Nytén, A. Abouimrane, M. Armand, T. Gustafsson, J.O. Thomas, Electrochem. Commun. 7 (2005) 156–160.
[2] R. Dominko, M. Bele, M. Gaberšček, A. Meden, M. Remškar, J. Jamnik, Electrochem. Commun. 8 (2006) 217–222.
[3] M.E.A. de Dompablo, M. Armand, J.M. Tarascon, U. Amador, Electrochem. Commun. 8 (2006) 1292–1298.
[4] M.S. Islam, R. Dominko, C. Masquelier, C. Sirisopanaporn, A.R. Armstrong, P.G. Bruce, J. Mater. Chem. 21 (2011) 9811–9818.
[5] A. Kojima, T. Kojima, M. Tabuchi, T. Sakai, J. Electrochem. Soc. 159 (2012) A532–A537.
[6] V. Aravindan, K. Karthikeyan, K.S. Kang, W.S. Yoon, W.S. Kim, Y.S. Lee, J. Mater. Chem. 21 (2011) 2470–2475.
[7] I. Belharouak, A. Abouimrane, K. Amine, J. Phys. Chem. C 113 (2009) 20733–20737.
[8] M.E.A. de Dompablo, R. Dominko, J.M.G. Amores, L. Dupont, G. Mali, H. Ehrenberg, J. Jamnik, E. Moran, Chem. Mater. 20 (2008) 5574–5584.
[9] S. Zhang, Y. Li, G. Xu, S. Li, Y. Lu, O. Toprakci, X. Zhang, J. Power Sources 213 (2012) 10–15.
[10] V. Aravindan, K. Karthikeyan, S. Ravi, S. Amaresh, W.S. Kim, Y.S. Lee, J. Mater. Chem. 20 (2010) 7340–7343.
[11] S. Luo, M. Wang, W. Sun, Ceram. Int. 38 (2012) 4325–4329.
[12] D.M. Kempaiah, D. Rangappa, I. Honma, Chem. Commun. 48 (2012) 2698–2700.
[13] D. Rangappa, K.D. Murukanahally, T. Tomai, A. Unemoto, I. Honma, Nano Lett. 12 (2012) 1146–1151.
[14] T. Muraliganth, K.R. Stroukoff, A. Manthiram, Chem. Mater. 22 (2010) 5754–5761.
[15] Y.-X. Li, Z.-L. Gong, Y. Yang, J. Power Sources 174 (2007) 528–532.
[16] X. Yan, G. Yang, J. Liu, Y. Ge, H. Xie, X. Pan, R. Wang, Electrochim. Acta 54 (2009) 5770–5774.
[17] R. Kostecki, B. Schnyder, D. Alliata, X. Song, K. Kinoshita, R. Kötz, Thin Solid Films 396 (2001) 36–43.
[18] C. Deng, S. Zhang, B.L. Fu, S.Y. Yang, L. Ma, Mater. Chem. Phys. 120 (2010) 14–17.
[19] R. Dominko, M. Bele, A. Kokalj, M. Gaberscek, J. Jamnik, J. Power Sources 174 (2007) 457–461.
[20] R. Dominko, J. Power Sources 184 (2008) 462–468.
[21] K. Karthikeyan, V. Aravindan, S.B. Lee, I.C. Jang, H.H. Lim, G.J. Park, M. Yoshio, Y.S. Lee, J. Power Sources 195 (2010) 3761–3764.
[22] V. Aravindan, S. Ravi, W.S. Kim, S.Y. Lee, Y.S. Lee, J. Colloid Interface Sci. 355 (2011) 472–477.
[23] M.E. Arroyo y de Dompablo, U. Amador, J.M. Gallardo-Amores, E. Morán, H. Ehrenberg, L. Dupont, R. Dominko, J. Power Sources 189 (2009) 638–642.
[24] V. Aravindan, K. Karthikeyan, S. Amaresh, Y.S. Lee, J. Electrochem. Soc. 14 (2011) A33–A35.
[25] W. Liu, Y. Xu, R. Yang, J. Alloys Compd. 480 (2009) L1–L4.
[26] A. Kokalj, R. Dominko, G. Mali, A. Meden, M. Gaberscek, J. Jamnik, Chem. Mater. 19 (2007) 3633–3640.
[27] X. Kong, T. Mei, Z. Xing, N. Li, Z. Yuan, Y. Zhu, Y. Qian, Int. J. Electrochem. Sci. 7 (2012) 5565–5573.